



RESEARCH

Open Access



# Oral epithelial dysplasia detection and grading in oral leukoplakia using deep learning

Jiakuan Peng<sup>1,3</sup>, Ziang Xu<sup>1</sup>, Hongxia Dan<sup>1</sup>, Jing Li<sup>1</sup>, Jiongke Wang<sup>1</sup>, Xiaobo Luo<sup>1</sup>, Hao Xu<sup>1\*</sup> , Xin Zeng<sup>1\*</sup>  and Qianming Chen<sup>2</sup>

## Abstract

**Background** The grading of oral epithelial dysplasia is often time-consuming for oral pathologists and the results are poorly reproducible between observers. In this study, we aimed to establish an objective, accurate and useful detection and grading system for oral epithelial dysplasia in the whole-slides of oral leukoplakia.

**Methods** Four convolutional neural networks were compared using the image patches from 56 whole-slide of oral leukoplakia labeled by pathologists as the gold standard. Sequentially, feature detection models were trained, validated and tested with 1,000 image patches using the optimal network. Lastly, a comprehensive system named E-MOD-plus was established by combining feature detection models and a multiclass logistic model.

**Results** EfficientNet-B0 was selected as the optimal network to build feature detection models. In the internal dataset of whole-slide images, the prediction accuracy of E-MOD-plus was 81.3% (95% confidence interval: 71.4–90.5%) and the area under the receiver operating characteristic curve was 0.793 (95% confidence interval: 0.650 to 0.925); in the external dataset of 229 tissue microarray images, the prediction accuracy was 86.5% (95% confidence interval: 82.4–90.0%) and the area under the receiver operating characteristic curve was 0.669 (95% confidence interval: 0.496 to 0.843).

**Conclusions** E-MOD-plus was objective and accurate in the detection of pathological features as well as the grading of oral epithelial dysplasia, and had potential to assist pathologists in clinical practice.

**Keywords** Oral leukoplakia, Oral epithelial dysplasia, Whole-slide image, Tissue microarray, Computational pathology, Deep learning

\*Correspondence:

Hao Xu  
hao.xu@scu.edu.cn  
Xin Zeng  
zengxin22@163.com

<sup>1</sup>State Key Laboratory of Oral Diseases, National Clinical Research Center for Oral Diseases, Research Unit of Oral Carcinogenesis and Management,

Chinese Academy of Medical Sciences, West China Hospital of Stomatology, Sichuan University, Chengdu Sichuan, China

<sup>2</sup>Key Laboratory of Oral Biomedical Research of Zhejiang Province, Affiliated Stomatology Hospital, Zhejiang University School of Stomatology, Hangzhou, Zhejiang, China

<sup>3</sup>Department of Stomatology, North Sichuan Medical College, Nanchong, Sichuan, China



© The Author(s) 2024. **Open Access** This article is licensed under a Creative Commons Attribution 4.0 International License, which permits use, sharing, adaptation, distribution and reproduction in any medium or format, as long as you give appropriate credit to the original author(s) and the source, provide a link to the Creative Commons licence, and indicate if changes were made. The images or other third party material in this article are included in the article's Creative Commons licence, unless indicated otherwise in a credit line to the material. If material is not included in the article's Creative Commons licence and your intended use is not permitted by statutory regulation or exceeds the permitted use, you will need to obtain permission directly from the copyright holder. To view a copy of this licence, visit <http://creativecommons.org/licenses/by/4.0/>. The Creative Commons Public Domain Dedication waiver (<http://creativecommons.org/publicdomain/zero/1.0/>) applies to the data made available in this article, unless otherwise stated in a credit line to the data.

## Background

Oral leukoplakia (OLK) is defined as white plaques or patches that cannot be wiped out of oral mucosa having excluded other known diseases by histopathology examination [1]. OLK is one of the most common oral potentially malignant disorders (OPMDs) and OLK has an appropriate malignant transformation rate of 1.1%~40.8% [2]. One of the most important indicators of the malignant transformation of OLK is oral epithelial dysplasia (OED) [3]. OED is a pathology term which is defined as abnormal architectural and cytological changes within mucosal epithelium of the oral cavity [4]. The presence of OED in OLK correlates with an increased risk of progression to carcinoma, and the higher degree of OED, the higher risk of progression [4]. Most of the time, the severity of OED is divided into three levels (mild, moderate and severe dysplasia) according to the World Health Organization (WHO) criteria (2022 version) [5]. Although there is a binary grading system mentioned by the criteria, the validation of this system against malignant transformation remains outstanding, limiting its application [6, 7]. The 3-tiered grading criteria focus on the range or affected layers of certain pathological features, including architectural and cytological features [5]. There were significant changes of pathological features from the 2017 to the 2022 version [5, 8, 9]. Notably, the 2017 version included 16 features, whereas the 2022 version had 11 additional features [5, 8]. The added features were “altered keratin pattern for oral sub-site”, “verrucous or papillary architecture”, “extension of changes along minor gland ducts”, “sharply defined margin to changes”, “multiple different patterns of dysplasia”, “multifocal or skip lesions”, “expanded proliferative compartment”, “basal cell clustering/nesting”, “single cell keratinization”, “apoptotic mitoses”, “increased nuclear size” [5]. If there is no presence of OED in OLK, the diagnosis of OLK is often given as hyperplasia or nondysplasia [10]. Currently, the detection and grading of OED severity is poorly reproducible between observers. One more obstacle that makes OED grading difficult is that visual inspection of tissue slides is a repetitive and time-consuming task for pathologists [11]. With the need of precision medicine increasing, early detection and grading of OED in OLK patients has become critical [12]. A more objective OED detection and grading approach could be beneficial to oral pathologists and OLK patients.

Deep learning algorithms, especially convolutional neural networks (CNNs), can extract basic features of images that contain rich information, for example, from whole-slide images (WSIs). Therefore, CNNs have been used in a wide range of medical image analysis tasks, especially in cancer diagnosis [11, 13–15], molecular subtype classification [11, 16–19] and survival prediction [16, 20–23]. In recent years, several studies have explored

the effect of deep learning algorithms on the prediction of OED from OPMD whole-slide images. One of the studies focused their work on predicting the severity of OED using only one CNN model and the accuracy of their CNN model reached 89.3% in an internal test dataset, at the patch-level [24]. A similar work compared two CNNs, DeepLabv3+ and UNet++, revealing that DeepLabv3+ achieved an accuracy of 93.3% [25]. In a related study, seven CNNs were utilized on OED datasets annotated with binary grading system, resulting in EfficientB0 having comparable metrics and the lowest loss among all CNNs [26]. However, the pathological features of OED, which are of great importance to OED grading, were ignored in previous studies. In a recent work, peri-epithelial lymphocytes were used to predict the malignant transformation of OED [27], but those features were still not taken into account. Furthermore, there is no convenient application that could assist pathologists in clinical practice.

In this study, we aimed to apply computational pathology methods including deep learning algorithms to OED detection and grading in OLK whole-slide images, in order to establish an objective, accurate and useful computational detection and grading system for OED.

## Methods

### Data acquisition

This study was approved by the Ethics Committee of West China Hospital of Stomatology, Sichuan University (WCHSIRB-D-2022-006). In this observational study, we collected diagnostic slides of OLK patients from oral medicine department of West China Hospital of Stomatology between 2013 and 2018. The patients were included based on the following criteria: (a) age > 18 years; (b) suspicion of OLK through clinical examination; and (c) confirmation of OLK through histopathological examination. There were 56 WSIs of 56 OLK patients that were included in this study. Additionally, we collected four OLK tissue microarrays (TMAs) from Chinese Academy of Medical Sciences Research Unit of Oral Carcinogenesis and Management. The TMAs included 229 samples of 93 OLK patients between 2004 and 2014, since some patients had multiple OLK lesions and all available tissue samples from different lesions of the same patient were included in this study. Slide preparations were completed in oral pathology department of West China Hospital of Stomatology and Chinese Academy of Medical Sciences Research Unit of Oral Carcinogenesis and Management, respectively. All slides were crafted from formalin-fixed paraffin-embedded tissue, and were hematoxylin & eosin stained. Whole-slide images were scanned using Leica APERIO VERSA 8 FL scanner and Aperio ImageScope software.

Dysplasia annotations were performed on the 56 WSIs and 229 tissue microarray images and were completed by two oral pathologists with 20-year experience who were blind to any clinical information of the patients, following the WHO criteria (2017 version) [8]: mild dysplasia can be defined by cytological changes limited to the basal third, moderate dysplasia by extension into the middle third, severe dysplasia by extension into the upper third,

and the presence of architectural changes may increase the level. Any disagreement between the two observers was solved by an expert oral pathologist with 30-year experience. There were four labels given to 56 whole-slide images: hyperplasia, mild dysplasia, moderate dysplasia and severe dysplasia. A typical example of these labels is shown in Fig. 1A.

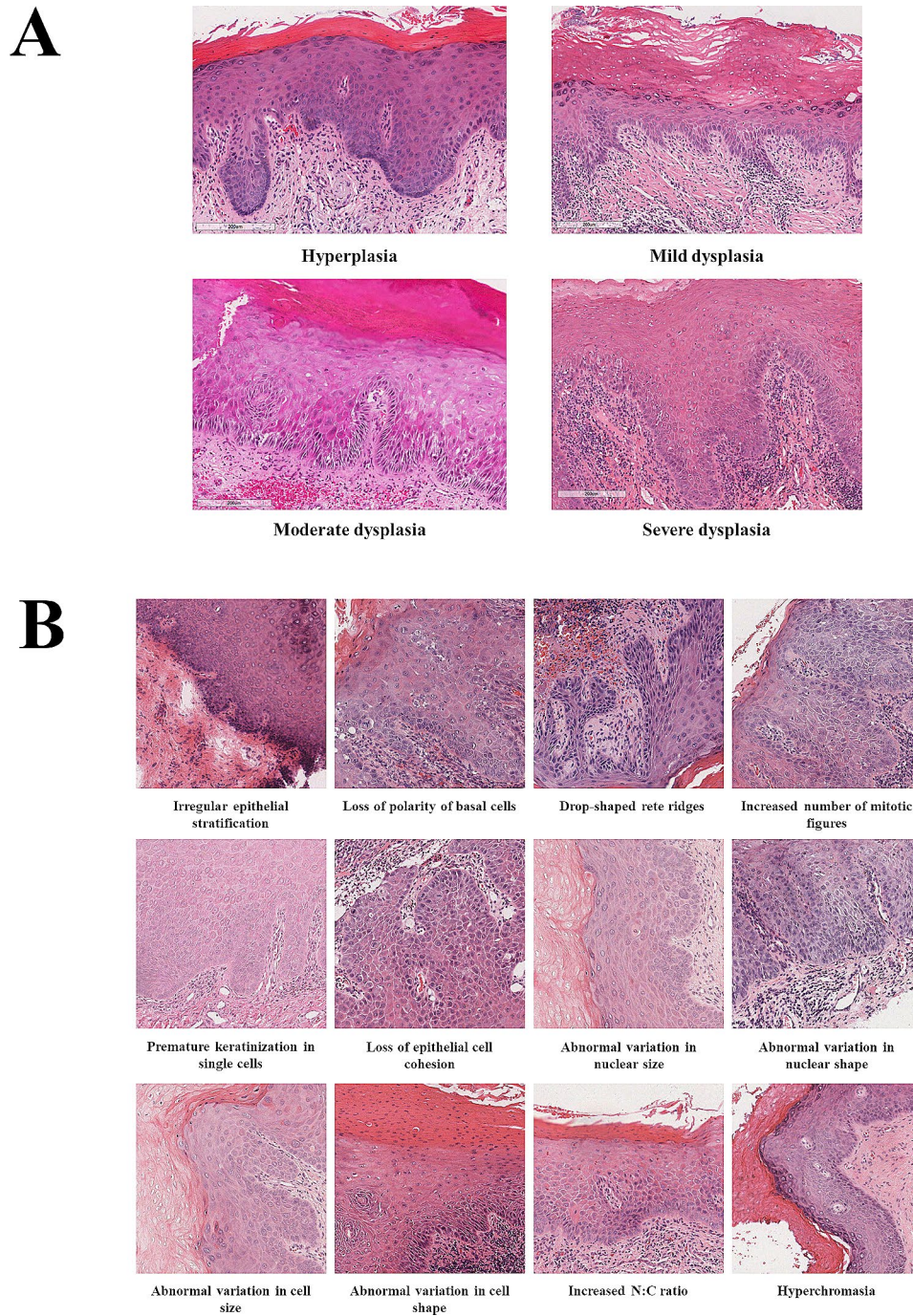


**Fig. 1** Example images of this study. **(A)** hyperplasia, mild dysplasia, moderate dysplasia, severe dysplasia in oral leukoplakia; **(B)** 12 pathological features of oral epithelial dysplasia which were included in this study

Annotations with “yes” or “no” to 16 OED pathological features were also completed by two oral pathologists with 20-year experience who were blind to any clinical information of the patients, following WHO criteria (2017 version). Any disagreement between two observers was solved by an expert oral pathologist with 30-year experience. There were 1,000 image patches (images originated from whole-slides) with annotation for each pathological feature. Pathological features which had a positive frequency less than 5 were excluded. Four pathological features were removed: abnormally superficial mitotic figures, keratin pearls within rete ridges, atypical mitotic figures, increased number and size of nucleoli. A typical example of these pathological features is shown in Fig. 1B.

### Image preprocessing

We applied non-overlapping image tiling to the slides and microarrays to split images into patches with Python module Openslide 1.1.1. Patches that contained over 50% background pixels (brightness > 220/255) were excluded [11]. To test the effect of differently scaled image inputs, we attempted to train networks using two different resolutions (224 pixels & 512 pixels) [16, 21] and two different magnifications. (10× & 20×) [16, 28] Through this process a total number of approximately 208,000 image patches were generated (approximately 161,000 WSI patches and approximately 47,000 TMA patches) (details are shown in Supplementary Table 1). The patches were labeled using the same labels as the parent slides. The size of 1000 images with pathological feature annotation was 224 pixels.

### Model training and validation

Two sorts of deep learning models were trained and validated: OED grading models and OED feature detection models.

For OED grading models, we evaluated four CNNs: ResNet-50 [29], Inception-V4 [30], ShuffleNet-V2 [31] and EfficientNet-B0 [32], to select the best network for OED grading. Grid search strategy was applied to the model selection procedure [33]. All networks were trained from scratch using randomized initial weights, with a mini-batch size of 80. The maximum number of epochs was set to 100 for every model. A model was selected only if it reached the lowest cross entropy loss in the validation dataset. The RMSprop (root mean squared propagation) optimizer was used as the optimizer of stochastic gradient descent algorithm and the learning rate was set to  $1 \times 10^{-4}$  [34]. The patches were divided into a train set of 60% patches, a validation set of 15% and a test set of 25%.

Following CNN selection, we used the best CNN to train OED feature detection models from scratch. As the

number of images with pathological feature annotation was relatively small, the maximum number of epochs was set to 200, and the learning rate of RMSprop was set to  $1 \times 10^{-6}$ , to prevent gradient explosion [35]. The other parameters remained unchanged during the training of OED feature detection models. Image distribution was in concordance with OED grading models, as 60% for train, 15% for validation and 25% for test.

Model training and validation were implemented on a workstation with four NVIDIA Tesla K80 graphics processing units, using Python 3.6.8 with modules TensorFlow 2.1.0, Openslide 1.1.1, Scikit-learn 0.23.1 and relative dependencies.

### Establishment of the comprehensive detection and grading system

The fully connected layers of OED feature detection models were removed, and the activation scores (range: 0~1) were extracted from them. These scores represent the probability of positive predictions of the pathological features at the patch-level. To better interpret the scores, we amplified them 100 times (range: 0~100). Slide-level scores were calculated using an average of all the patch-level scores included in a single whole-slide image. Slide-level scores were used as the variables of a multiclass logistic model (ordinal logistic model) for OED grading:

$$\text{logit} \left( \sum_{i=1}^n p_i \right) = \alpha_n + \sum_{j=1}^{12} \beta_j \times \text{Score}_j \quad (1)$$

The performance of this model was evaluated in 56 OLK whole-slides as well as 229 TMA images, at the slide level. Additionally, the performance of this model was compared with 3 junior oral pathologists who have less than 5 years' experience. The junior pathologists were assigned to conduct OED grading following the WHO criteria (2017 version) as well. The establishment of this comprehensive detection and grading system can be summarized in Fig. 2.

### Development of a detection and grading application

We used PyQt5 to develop an application for OED grading and OED feature detection. To integrate the prediction results, heatmaps were generated using the values of categorical softmax function. Then we assembled all foreground patches (background pixels < 50%) according to the original spatial coordinates.

### Statistical analysis

The baseline information of OLK patients was tested using Kruskal-Wallis test (continuous variables) or Fisher's test (categorical variables), two-tailed *P*value less than 0.05 was considered significant. The diagnostic

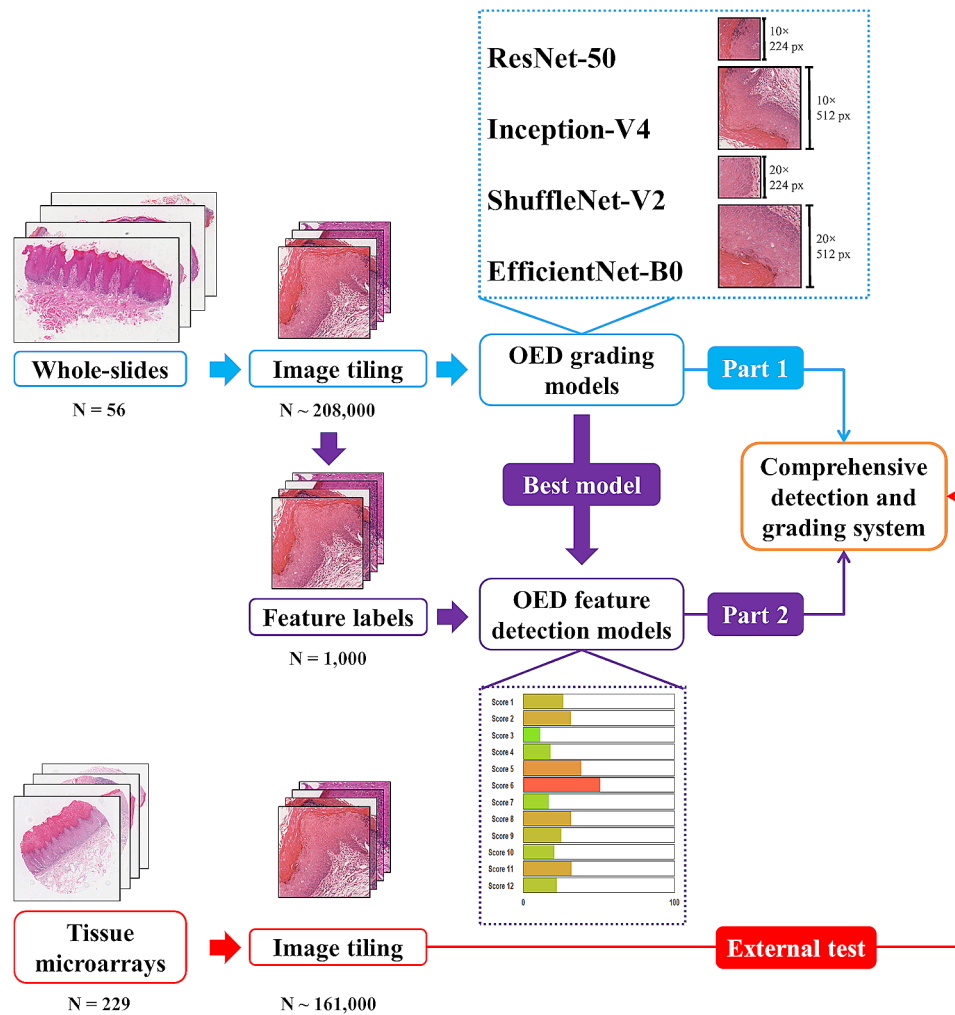


**Fig. 2** The development of the OED grading system. OED: oral epithelial dysplasia

accuracy indicators including accuracy, sensitivity, specificity and area under the receiver operating characteristic curve (AUC) in test datasets were used to assess the performances of trained networks. The confident intervals (CIs) of these metrics were calculated using the bootstrapping method. As the labels had four categories, these metrics were calculated as averages. The accuracy and AUC were the primary criteria for evaluation. All the statistical analysis was performed with Python 3.6.8 and R 3.6.1.

**Results**

**The baseline of OLK patients**

Among OLK patients whose slide images were used for training, there were 22 male patients and 34 female patients; an average age of the patients was 56.9 ( $\pm 11.8$ ) years; and the most frequently affected anatomic site was tongue, followed by buccal mucosa, gingiva and floor of mouth. Overall, the baseline information was in consistency with the general clinical epidemiological profile of

OLK, and the distribution was not significantly biased (Table 1). Among TMA cases, there were 42 male cases and 51 female cases; an average age of the cases was 58.5 ( $\pm 11.8$ ) years; and the most frequently affected anatomic site was buccal mucosa, followed by tongue, palate, gingiva and floor of mouth. The affected sites were absent in 36 (15.7%) of 229 TMA images (Table 2).

**Selection of CNNs**

In the test datasets, four CNNs performed well when trained with 20 $\times$ , 224-pixel patches. EfficientNet-B0 trained with 20 $\times$ , 224-pixel patches was the best model in comparison with others (average accuracy=97.5%, Table 3). Furthermore, we calculated the AUCs of 16 models, and found that EfficientNet-B0 trained with 20 $\times$ , 224-pixel patches outperformed others as well (average AUC=0.993, Table 3). The best parameters of EfficientNet-B0 and Inception-V4 were 20 $\times$ , 224 pixels, and the best parameters of ResNet-50 and ShuffleNet-V2 were 10 $\times$ , 224 pixels.

**Table 1** Baseline information of OLK patients

	Hyperplasia	Mild dysplasia	Moderate dysplasia	Severe dysplasia	Total	P
Number of slides	16	21	12	7	56	
Sex						<b>0.48</b>
Male	8 (50.0%)	8 (38.1%)	5 (41.7%)	1 (14.3%)	22 (39.3%)	
Female	8 (50.0%)	13 (61.9%)	7 (58.3%)	6 (85.7%)	34 (60.7%)	
Age	53.7 ± 13.4	57.7 ± 10.0	57.2 ± 13.8	61.7 ± 9.8	56.9 ± 11.8	<b>0.56</b>
Site						<b>0.65</b>
Buccal mucosa	4 (25.0%)	8 (38.1%)	4 (33.3%)	4 (57.1%)	20 (35.7%)	
Tongue	8 (50.0%)	11 (52.4%)	8 (66.7%)	3 (42.9%)	30 (53.6%)	
Gingiva	3 (18.8%)	2 (9.5%)	0 (0.0%)	0 (0.0%)	5 (8.9%)	
Floor of mouth	1 (6.2%)	0 (0.0%)	0 (0.0%)	0 (0.0%)	1 (1.8%)	

Categorical variables were demonstrated as frequencies and percentages, and were tested by Fisher’s test; continuous variables were demonstrated as averages and standard deviations, and were tested by Kruskal-Wallis test. OLK: oral leukoplakia

**Table 2** Baseline information of TMA cases

	Hyperplasia	Mild dysplasia	Moderate dysplasia	Severe dysplasia	Total	P
Number of slides	124	43	51	11	229	
Sex						<b>0.55</b>
Male	61 (49.2%)	18 (41.9%)	20 (39.2%)	6 (54.5%)	105 (45.9%)	
Female	63 (50.8%)	25 (58.1%)	31 (60.8%)	5 (45.5%)	124 (54.1%)	
Age	57.8 ± 12.2	59.0 ± 13.0	60.8 ± 10.0	58.8 ± 9.6	58.7 ± 11.8	<b>0.46</b>
Site						<b>&lt; 0.001</b>
Buccal mucosa	57 (46.0%)	29 (67.4%)	18 (35.3%)	7 (63.4%)	111 (48.5%)	
Tongue	33 (26.6%)	9 (20.9%)	12 (23.5%)	1 (9.1%)	55 (24.0%)	
Gingiva	9 (7.3%)	2 (4.7%)	0 (0.0%)	0 (0.0%)	11 (4.8%)	
Floor of mouth	0 (0.0%)	0 (0.0%)	0 (0.0%)	2 (18.2%)	2 (0.9%)	
Palate	14 (11.3%)	0 (0.0%)	0 (0.0%)	0 (0.0%)	14 (6.1%)	
Missing	11 (8.9%)	3 (7.0%)	21 (41.2%)	1 (9.1%)	36 (15.7%)	

Categorical variables were demonstrated as frequencies and percentages, and were tested by Fisher’s test; continuous variables were demonstrated as averages and standard deviations, and were tested by Kruskal-Wallis test. TMA: tissue microarray

**Table 3** The performances of convolutional neural networks

	Accuracy (%)	95% CI (%)	AUC	95% CI
ShuffleNet-V2				
224 px & 10x	91.1	(90.5, 91.8)	0.957	(0.952, 0.962)
224 px & 20x	89.0	(88.7, 89.4)	0.957	(0.955, 0.959)
512 px & 10x	72.6	(70.3, 75.0)	0.729	(0.692, 0.763)
512 px & 20x	80.8	(79.8, 81.8)	0.809	(0.794, 0.823)
ResNet-50				
224 px & 10x	90.6	(89.9, 91.3)	0.954	(0.949, 0.960)
224 px & 20x	88.0	(87.6, 88.4)	0.930	(0.926, 0.933)
512 px & 10x	72.6	(70.3, 75.0)	0.633	(0.598, 0.666)
512 px & 20x	85.1	(84.2, 86.0)	0.894	(0.884, 0.903)
Inception-V4				
224 px & 10x	93.8	(93.3, 94.4)	0.979	(0.976, 0.983)
224 px & 20x	94.9	(94.6, 95.1)	0.987	(0.986, 0.988)
512 px & 10x	75.2	(73.0, 77.5)	0.603	(0.565, 0.640)
512 px & 20x	82.5	(81.5, 83.5)	0.772	(0.755, 0.788)
EfficientNet-B0				
224 px & 10x	92.8	(92.3, 93.4)	0.966	(0.961, 0.971)
224 px & 20x	97.5	(97.3, 97.6)	0.993	(0.992, 0.994)
512 px & 10x	76.6	(74.4, 78.9)	0.741	(0.709, 0.774)
512 px & 20x	89.6	(88.8, 90.4)	0.928	(0.919, 0.937)

CI: confidence interval; AUC: area under the receiver operating characteristic curve; px: pixel

Therefore, we selected EfficientNet-B0 as the best CNN for OED grading, and referred to it as E-MOD (EfficientNet-B0 Model for OED Diagnosis). E-MOD had an average accuracy of 97.5% (95% CI: 97.3%~97.6%), an average AUC of 0.993 (95% CI: 0.992~0.994), an average sensitivity of 94.7% (95% CI: 94.2%~95.3%), and an average specificity of 98.3% (95% CI: 98.1%~98.4%).

We used TMA images to test the robustness of E-MOD. At the patch-level, E-MOD had an average accuracy of 90.9% (95% CI: 90.2%~91.6%) and an average AUC of 0.875 (95% CI: 0.865~0.885). The predictions at the slide-level were calculated according to the maximum proportion of each category. At the slide-level, E-MOD had an average accuracy of 63.5% (95% CI: 57.4%~69.6%), an average AUC of 0.673 (95% CI: 0.484~0.824), an average sensitivity of 86.1% (95% CI: 81.2%~90.6%), and an average specificity of 64.0% (95% CI: 56.5%~71.0%).

**Testing pathological feature detection models**

The performances of 12 pathological feature detection models are shown in Table 4. The median accuracy of the models was 79.7% and the median AUC was 0.766, suggesting that EfficientNet-B0 was accurate in the detection of OED features. After training 12 pathological feature detection models with EfficientNet-B0, the softmax activation scores were extracted from the models. Therefore, we obtained 12 scores as the variables of a multiclass logistic model.

**Establishment of a comprehensive grading system**

In the internal test dataset, the multiclass logistic model had an average accuracy of 81.3% (95% CI: 71.4%~90.5%), an average AUC of 0.793 (95% CI: 0.650~0.925, Fig. 3A), an average sensitivity of 61.6% (95% CI: 33.3%~85.4%), and an average specificity of 86.0% (95% CI: 76.2%~94.7%). We also used TMA images to test the robustness of the model. It had an average accuracy of 86.5% (95% CI: 82.4%~90.0%), an average AUC of 0.669

(95% CI: 0.496~0.843, Fig. 3B), an average sensitivity of 70.6% (95% CI: 67.3%~73.9%), and an average specificity of 79.4% (95% CI: 76.1%~82.8%). The average accuracy of the model (86.5%) was significantly higher than E-MOD (63.5%). Furthermore, this model demonstrated superior performance over three junior oral pathologists in terms of OED grading. In the internal test dataset, it achieved the highest accuracy and AUC. Meanwhile, in the TMA dataset, it exhibited the highest values for almost all metrics, including accuracy, AUC, and sensitivity (Supplementary Table 2).

Finally, we combined the model and E-MOD to establish a comprehensive grading system for OED, which was named E-MOD-plus. Meanwhile, an application of E-MOD-plus was developed, as an auxiliary tool for oral pathologist. As Fig. 4 shows, E-MOD-plus can not only accurately predict OED level at the whole-slide level, but also predict the presence of OED features.

**Discussion**

OED grading is crucial to the prognosis of OLK, and could also influence prevention or treatment strategies [4]. While the complexity of the OED grading criteria makes the job heavy to oral pathologists, an accurate and objective computational model could be helpful for improving the efficiency of OED grading.

In our study, four CNNs were firstly evaluated using four differently scaled image inputs. All of them reached promising performances, especially EfficientNet-B0. When trained with 20x, 224-pixel patches, EfficientNet-B0 model (E-MOD) achieved the highest accuracy and AUC, at the patch-level. The selection of CNN is an important factor to develop a computer-aided grading system. ResNet-50 and Inception-V4 are two popular networks for medical image analysis due to high accuracy and robustness, but the training process is usually slow because of the complexity of their structures [29, 30]. ShuffleNet-V2 is a significantly faster network designed

**Table 4** The performances of 12 pathological feature detection models

Pathological Feature	Accuracy (%) (95% CI)	AUC (95% CI)
Irregular epithelial stratification	78.2(67.3~89.1)	0.768 (0.576~0.930)
Loss of polarity of basal cells	79.3 (62.1~93.1)	0.722 (0.578~0.813)
Drop-shaped rete ridges	86.9 (78.7~95.1)	0.900 (0.814~0.967)
Increased number of mitotic figures	81.7 (71.7~91.7)	0.806 (0.671~0.927)
Premature keratinization in single cells	96.9 (92.2~98.4)	0.734 (0.544~0.856)
Loss of epithelial cell cohesion	98.4 (93.4~98.4)	0.983 (0.948~1.000)
Abnormal variation in nuclear size	67.6 (51.4~81.1)	0.725 (0.612~0.818)
Abnormal variation in nuclear shape	78.9 (65.8~92.1)	0.776 (0.600~0.923)
Abnormal variation in cell size	80.0 (68.9~91.1)	0.883 (0.737~0.993)
Abnormal variation in cell shape	88.6 (79.5~97.7)	0.764 (0.646~0.876)
Increased N: C ratio	62.5 (51.5~79.5)	0.742 (0.604~0.796)
Hyperchromasia	65.4 (51.9~78.8)	0.679 (0.587~0.759)

AUC: area under the curve; CI: confidence interval

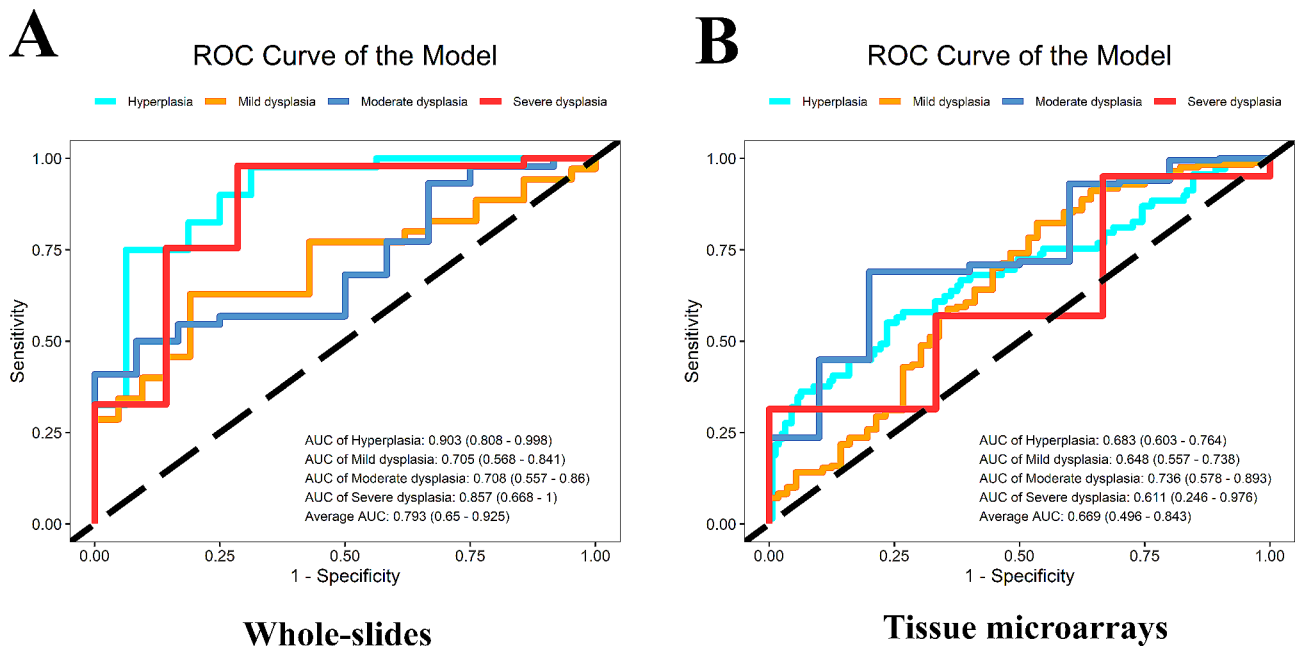


**Fig. 3** (A) The ROC curves of the multiclass logistic model in whole-slides. (B) The ROC curves of the multiclass logistic model in tissue microarrays. ROC: receiver operating characteristic; AUC: area under the curve

for mobile devices, but the accuracy is relatively lower [31]. EfficientNet-B0 is an advanced one that combines high accuracy and high speed. The essence of EfficientNet-B0 is to systematically scale depth, width and resolution, to achieve a balance of accuracy and efficiency [32]. Therefore, EfficientNet-B0 was selected as the best model for OED grading.

However, in the TMA dataset, E-MOD had an average accuracy of 63.5%, and an average AUC of 0.673, at the slide level. These results suggest that using the proportions of patches to directly integrate the classification of a deep learning model was probably not a proper approach. Hence, we considered combining the detection of OED features to assist slide-level prediction, since this process is crucial to OED grading in the routine diagnosing workflow. Now that EfficientNet-B0 was highly accurate at the patch level (including TMA patches), we utilized EfficientNet-B0 to train feature detection models, and extracted the values of activation functions as scores. The scores were finally integrated in a multiclass logistic model and it achieved better performance than E-MOD. The average accuracy of the multiclass logistic model (86.5%) was significantly higher than E-MOD (63.5%), though there is no significant differences between the AUC. These results suggest that the combination of OED features is more effective than mere whole-slides. In comparison with junior oral pathologists, this model exhibited decent performances. Notably, this model achieved the highest accuracy and AUC in both test datasets. This not only signifies its consistently high-level performance

with diverse slides, but it also reinforces the potential for computational pathology applications in OED grading.

Finally, E-MOD-plus, an OED grading application was developed, by combining E-MOD and the multiclass logistic model based on the scores of OED features. E-MOD-plus was accurate, objective and user-friendly. It is noteworthy that the highlighted patches, which are indicative of high diagnostic value in the prediction map, have the potential to play a decisive role in OED grading. These regions have an increased possibility of containing OED pathological features, merit thorough review by pathologists if they cannot grade OED quickly. E-MOD-plus could be positioned as an adjunct to pathologists, especially in the initial screening and re-evaluating stages. During the initial screening stage, E-MOD-plus can grade batches of slides with ease, accelerating the OED grading process. When grading complex cases, pathologists are encouraged to review the heatmaps generated by the model, to locate regions where significant pathological features of OED may be present. This collaborative approach leverages the strengths of both human expertise and machine efficiency, creating a synergy that enhances the overall OED grading process.

This study was performed as a preliminary investigation of OLK computational histopathology which had several limitations. First of all, the reference grading criteria of OED needs to be updated. As substantial modifications were made to the pathological features in the WHO criteria (2022 version) [5], it is also necessary to evaluate the effect of added features if they are included in the model. Another limitation of our study was the



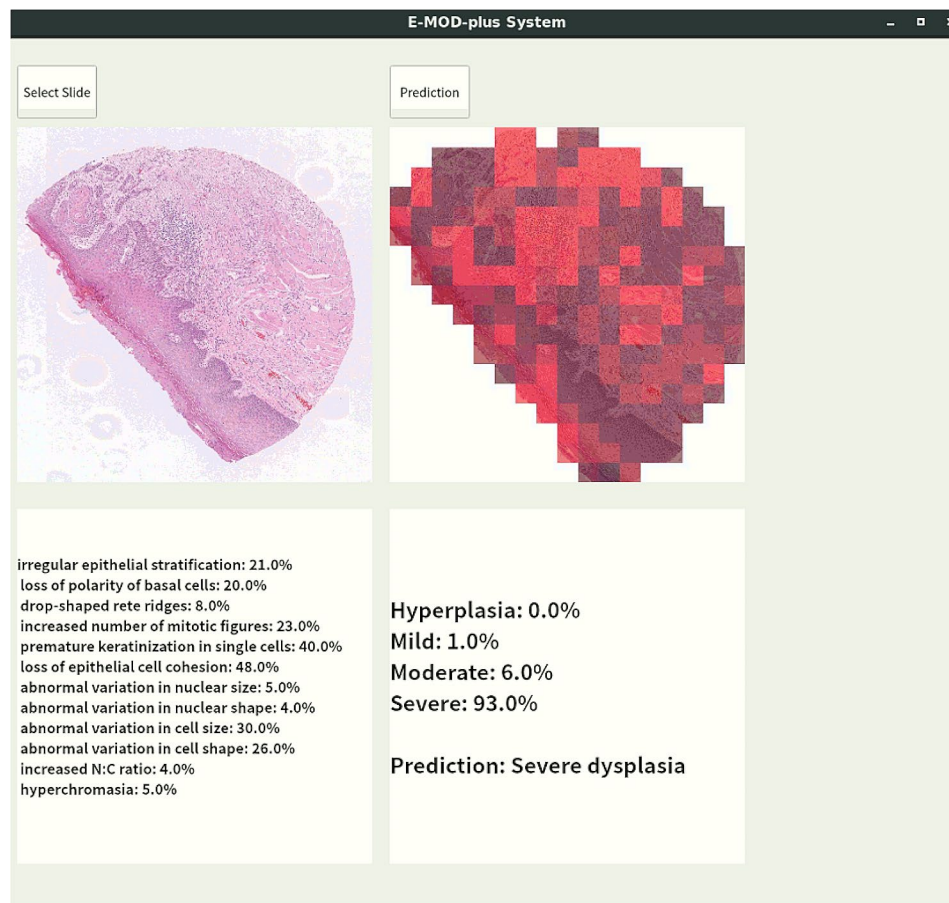


**Fig. 4** The interface of E-MOD-plus, the proposed detection and grading application of oral epithelial dysplasia. The upper left shows the input whole-slide image; the upper right shows a heatmap which marks a higher level of oral epithelial dysplasia with a brighter color; the lower left shows the probabilities of 12 pathological features; and the lower right shows a prediction of the whole-slide

relatively small sample size employed in the development and evaluation of E-MOD-plus. While the current dataset has provided valuable insights and a foundation for E-MOD-plus, its size constrains the generalizability of our findings. To address this limitation in future research, collaborative efforts with other research institutions and healthcare providers will be pursued to aggregate larger datasets, enabling a more comprehensive analysis and further validation of the model's performance. The next limitation was that we used parent labels to categorize patches, which can make the ground truth labels noisy. However, this is an obstacle in the advances of computational pathology [36]. An ideal solution to this problem is massive manual annotations of several expert oral pathologists, which is extremely time-consuming. In this study, the neural networks still showed powerful detection and grading performances, suggesting deep learning algorithms could partially overcome the disadvantage of imbalanced and noisy ground truth labels.

Moving forward, our focus lies in gathering comprehensive prognosis information on the subjects involved in the study. This approach will enable us to track the

progression of malignant transformation over time, providing better understanding of the relation between OED severity and malignant transformation. Moreover, we will utilize prognosis as an outcome for enhancing our model. By incorporating detailed prognostic data, our model can evolve beyond mere OED feature detection and OED grading, aiming to contribute meaningfully to the prediction of malignant transformation.

Last but not least, although our models reached satisfactory performances when trained from scratch, they are likely to be improved with transfer learning [37]. Transfer learning replaces randomized initial weights with ones from pretrained models using known datasets such as ImageNet [38]. It is believed that an increase in accuracy and a reduction in convergence time can be observed after applying transfer learning in model training [37, 39]. Therefore, we aimed to include transfer learning in grid search strategy in future studies.

## Conclusions

In conclusion, E-MOD-plus, the OED detection and grading system for OLK, was objective and accurate in the detection of OED pathological features as well as the grading of OED, and had potential to assist oral pathologists in clinical practice.

## Abbreviations

OLK	oral leukoplakia
OPMD	oral potentially malignant disorder
OED	oral epithelial dysplasia
WHO	World Health Organization
CNN	convolutional neural network
WSI	whole-slide image
TMA	tissue microarray
AUC	area under the curve
CI	confidence interval

## Supplementary Information

The online version contains supplementary material available at <https://doi.org/10.1186/s12903-024-04191-z>.

Supplementary Material 1

Supplementary Material 2

## Acknowledgements

We appreciate the hard work of all the pathologists who participated in our study.

## Author contributions

Jiakuan Peng: conceptualization, methodology, software, formal analysis, writing original draft, visualization. Ziang Xu: conceptualization, methodology, software, formal analysis, writing original draft. Hongxia Dan: resources, data curation, validation, supervision. Jing Li: resources, data curation, validation, supervision. Jiongke Wang: resources, data curation, validation, supervision, visualization. Xiaobo Luo: resources, data curation, validation, supervision, visualization. Hao Xu: conceptualization, methodology, formal analysis, writing review and editing, funding acquisition. Xin Zeng: conceptualization, writing review and editing, supervision, funding acquisition. Qianming Chen: conceptualization, supervision, project administration. All authors have read and approved the final manuscript.

## Funding

This study was supported by grants from the National Natural Science Foundation of China (U19A2005, 82001059, 81771081, 82370962), CAMS Innovation Fund for Medical Sciences (CIFMS, 2019-12 M-5-004 and 2020-I2M-C&T-A-023) and Research Funding for Talents Developing, West China Hospital of Stomatology, Sichuan University (RCDWJS2020-22), China.

## Data availability

The whole-slides and tissue microarrays are not publicly available in order to protect privacy of the patients, but are available from the corresponding author upon reasonable request. The source codes of E-MOD-plus are deposited at <https://github.com/chxhstatis/E-MOD-plus>.

## Declarations

### Ethics approval and consent to participate

This study was approved by the Ethics Committee of West China Hospital of Stomatology, Sichuan University (WCHSIRB-D-2022-006). We confirm that all methods were carried out in accordance with relevant guidelines and regulations, and that informed consent was obtained from all subjects.

### Consent for publication

Not applicable.

## Competing interests

The authors declare no competing interests.

Received: 7 March 2023 / Accepted: 27 March 2024

Published online: 09 April 2024

## References

- Warnakulasuriya S, Kujan O, Aguirre-Urizar JM, Bagan JV, Gonzalez-Moles MA, Kerr AR, et al. Oral potentially malignant disorders: a consensus report from an international seminar on nomenclature and classification, convened by the WHO collaborating centre for oral Cancer. *Oral Dis.* 2021;27(8):1862–80.
- Aguirre-Urizar JM, Lafuente-Ibanez de Mendoza I, Warnakulasuriya S. Malignant transformation of oral leukoplakia: systematic review and meta-analysis of the last 5 years. *Oral Dis.* 2021;27(8):1881–95.
- Warnakulasuriya S, Kovacevic T, Madden P, Coupland VH, Sperandio M, Odell E, et al. Factors predicting malignant transformation in oral potentially malignant disorders among patients accrued over a 10-year period in South East England. *J oral Pathol Medicine: Official Publication Int Association Oral Pathologists Am Acad Oral Pathol.* 2011;40(9):677–83.
- Odell E, Kujan O, Warnakulasuriya S, Sloan P. Oral epithelial dysplasia: Recognition, grading and clinical significance. *Oral Dis.* 2021;27(8):1947–76.
- Muller S, Tilakaratne WM. Update from the 5th Edition of the World Health Organization Classification of Head and Neck tumors: Tumours of the oral cavity and Mobile Tongue. *Head Neck Pathol.* 2022;16(1):54–62.
- Nankivell P, Williams H, Matthews P, Suortamo S, Snead D, McConkey C, et al. The binary oral dysplasia grading system: validity testing and suggested improvement. *Oral Surg Oral Med Oral Pathol Oral Radiol.* 2013;115(1):87–94.
- Warnakulasuriya S, Reibel J, Bouquot J, Dabelsteen E. Oral epithelial dysplasia classification systems: predictive value, utility, weaknesses and scope for improvement. *J oral Pathol Medicine: Official Publication Int Association Oral Pathologists Am Acad Oral Pathol.* 2008;37(3):127–33.
- El-Naggar AK, Chan JKC, Rubin Grandis J, Takata T, Slootweg PJ. WHO classification of head and neck tumours 2017.
- Woo SB. Oral epithelial dysplasia and Premalignancy. *Head Neck Pathol.* 2019;13(3):423–39.
- Tilakaratne WM, Jayasooriya PR, Jayasuriya NS, De Silva RK. Oral epithelial dysplasia: causes, quantification, prognosis, and management challenges. *Periodontol 2000.* 2019;80(1):126–47.
- Coudray N, Ocampo PS, Sakellaropoulos T, Narula N, Snuderl M, Fenyo D, et al. Classification and mutation prediction from non-small cell lung cancer histopathology images using deep learning. *Nat Med.* 2018;24(10):1559–67.
- Acs B, Rantalainen M, Hartman J. Artificial intelligence as the next step towards precision pathology. *J Intern Med.* 2020;288(1):62–81.
- Gecer B, Aksoy S, Mercan E, Shapiro LG, Weaver DL, Elmore JG. Detection and classification of cancer in whole slide breast histopathology images using deep convolutional networks. *Pattern Recogn.* 2018;84:345–56.
- Halicek M, Shahedi M, Little JV, Chen AY, Myers LL, Sumer BD, et al. Head and Neck Cancer detection in digitized whole-slide histology using Convolutional neural networks. *Sci Rep.* 2019;9(1):14043.
- Kriegsmann M, Haag C, Weis CA, Steinbuss G, Warth A, Zgorzelski C et al. Deep learning for the classification of small-cell and non-small-cell Lung Cancer. *Cancers.* 2020;12(6).
- Kather JN, Krisam J, Charoentong P, Luedde T, Herpel E, Weis C-A, et al. Predicting survival from colorectal cancer histology slides using deep learning: a retrospective multicenter study. *PLoS Med.* 2019;16(1):e1002730.
- Ali HR, Dariush A, Provenzano E, Bardwell H, Abraham JE, Iddawela M, et al. Computational pathology of pre-treatment biopsies identifies lymphocyte density as a predictor of response to neoadjuvant chemotherapy in breast cancer. *Breast cancer Research: BCR.* 2016;18(1):21.
- Sirinukunwattana K, Domingo E, Richman SD, Redmond KL, Blake A, Verrill C, et al. Image-based consensus molecular subtype (imCMS) classification of colorectal cancer using deep learning. *Gut.* 2021;70(3):544–54.
- Woerl AC, Eckstein M, Geiger J, Wagner DC, Daher T, Stenzel P, et al. Deep learning predicts molecular subtype of muscle-invasive bladder Cancer from conventional histopathological slides. *Eur Urol.* 2020;78(2):256–64.
- Courtillot P, Maussion C, Moarii M, Pronier E, Pilcer S, Sefta M, et al. Deep learning-based classification of mesothelioma improves prediction of patient outcome. *Nat Med.* 2019;25(10):1519–25.

21. Fu Y, Jung AW, Torne RV, Gonzalez S, Vöhringer H, Shmatko A et al. Pan-cancer computational histopathology reveals mutations, tumor composition and prognosis. *bioRxiv*. 2020:813543.
22. Mobadersany P, Yousefi S, Amgad M, Gutman DA, Barnholtz-Sloan JS, Velázquez Vega JE, et al. Predicting cancer outcomes from histology and genomics using convolutional networks. *Proc Natl Acad Sci*. 2018;115(13):E2970.
23. Skrede O-J, De Raedt S, Kleppe A, Hveem TS, Liestøl K, Maddison J, et al. Deep learning for prediction of colorectal cancer outcome: a discovery and validation study. *Lancet*. 2020;395(10221):350–60.
24. Gupta RK, Kaur M, Manhas J. Tissue level based Deep Learning Framework for early detection of dysplasia in oral squamous epithelium. *J Multimedia Inform Syst*. 2019;6(2):81–6.
25. Liu Y, Bilodeau E, Pollack B, Batmanghelich K. Automated detection of premalignant oral lesions on whole slide images using convolutional neural networks. *Oral Oncol*. 2022;134:106109.
26. Araujo ALD, Silva VMD, Moraes MC, de Amorim HA, Fonseca FP, Sant'Ana MSP, et al. The use of deep learning state-of-the-art architectures for oral epithelial dysplasia grading: a comparative appraisal. *J oral Pathol Medicine: Official Publication Int Association Oral Pathologists Am Acad Oral Pathol*. 2023;52(10):980–7.
27. Bashir RMS, Shephard AJ, Mahmood H, Azarmehr N, Raza SEA, Khurram SA, et al. A digital score of peri-epithelial lymphocytic activity predicts malignant transformation in oral epithelial dysplasia. *J Pathol*. 2023;260(4):431–42.
28. Tomita N, Abdollahi B, Wei J, Ren B, Suriawinata A, Hassanpour S. Attention-based deep neural networks for detection of cancerous and precancerous esophagus tissue on histopathological slides. *JAMA Netw Open*. 2019;2(11):e1914645.
29. He K, Zhang X, Ren S, Sun J. Deep Residual Learning for Image Recognition. *arXiv e-prints*. 2015;arXiv:1512.03385.
30. Szegedy C, Ioffe S, Vanhoucke V, Alemi A. Inception-v4, Inception-ResNet and the impact of residual connections on learning. *arXiv e-prints*. 2016;arXiv:160207261.
31. Zhang X, Zhou X, Lin M, Sun J. ShuffleNet: an extremely efficient convolutional neural network for Mobile devices. *arXiv e-prints*. 2017;arXiv:170701083.
32. Tan M, Le QV. EfficientNet. Rethinking Model Scaling for Convolutional Neural Networks. *arXiv e-prints*. 2019;arXiv:1905.11946.
33. Jobczyk M, Stawiski K, Kaszkowiak M, Rajwa P, Rozanski W, Soria F et al. Deep learning-based recalibration of the CUETO and EORTC Prediction Tools for recurrence and progression of non-muscle-invasive bladder Cancer. *Eur Urol Oncol*. 2021.
34. Campanella G, Hanna MG, Geneslaw L, Mirafior A, Werneck Krauss Silva V, Busam KJ, et al. Clinical-grade computational pathology using weakly supervised deep learning on whole slide images. *Nat Med*. 2019;25(8):1301–9.
35. Wilson DR, Martinez TR. The need for small learning rates on large problems. *IJCNN'01 International Joint Conference on Neural Networks Proceedings (Cat No01CH37222)*; 15–19 July 20012001. pp. 115-9 vol.1.
36. Abels E, Pantanowitz L, Aeffner F, Zarella MD, van der Laak J, Bui MM, et al. Computational pathology definitions, best practices, and recommendations for regulatory guidance: a white paper from the Digital Pathology Association. *J Pathol*. 2019;249(3):286–94.
37. Van Opbroek A, Achterberg HC, Vernooij MW, De Bruijne M. Transfer learning for image segmentation by combining Image Weighting and Kernel Learning. *IEEE Trans Med Imaging*. 2019;38(1):213–24.
38. Lu J, Behbood V, Hao P, Zuo H, Xue S, Zhang GQ. Transfer learning using computational intelligence: a survey. *Knowl-Based Syst*. 2015;80(1):14–23.
39. Nishio M, Sugiyama O, Yakami M, Ueno S, Kubo T, Kuroda T, et al. Computer-aided diagnosis of lung nodule classification between benign nodule, primary lung cancer, and metastatic lung cancer at different image size using deep convolutional neural network with transfer learning. *PLoS ONE*. 2018;13(7):e0200721.

### Publisher's Note

Springer Nature remains neutral with regard to jurisdictional claims in published maps and institutional affiliations.